Measuring Low Energy Nuclear Cross Sections using ICF

Mark Yuly, Stephen Padalino, Emma Bruce, Katelyn Cook, and Sarah Hull.

Why use ICF for nuclear science?

Inertial confinement fusion (ICF) is a relatively new tool for the study of fundamental nuclear science which offers the promise of allowing measurements that would be very difficult, if not impossible, to carry out using traditional accelerator techniques. Our goal for the project described here is to focus on designing nuclear physics experiments that could not be done using an accelerator, but for which ICF is uniquely suited. ICF has a several important characteristics which, if exploited, may allow nuclear physics measurements to be extended into new energy regions.

1. In thermonuclear reactions such as occur in an ICF implosion, macroscopic amounts of matter reach temperatures high enough for nuclear reactions to begin to occur, although the energies involved are still relatively low compared to the energies at which accelerator-based experiments are typically carried out. Even though the energies are very low for ICF, there are so many ions involved that even though the nuclear cross sections are tiny there is still a change of having a measurable yield. For example, a back-of-the-envelope estimate for the time required to measure the ^{7}Li(t,α)^{6}He reaction at 25 MeV using an accelerator, with a triton beam current of 1 μA, is about one month for 1000 reactions to occur. In contrast, as estimated below, a single OMEGA shot doped with 1% ^{7}Li could produce about 10^{6} reactions in less than 1 ns.

2. The high reaction rate that results from the short duration of the ICF burn, however, creates a strong radiation pulse that would make it very difficult to measure the small number of prompt reaction products that would be produced by these low cross section reactions. For example, a typical OMEGA laser shot might produce a prompt yield of 10^{13} neutrons in a pulse of around 100 ps duration [1].

3. Laboratories carrying out ICF research are equipped for working with tritium, which remains confined to the target chamber after the shot. Because of the radiological hazards associated with tritium contamination, presently nuclear reactions involving tritium beams are only studied using very low intensity secondary beams produced via ^{9}Be(α, t) (10^{6}/s) [2] at NSCL, in-flight heavy-ion fragmentation of ^{16}O (5×10^{6}) [3] at NSCL, or very low intensity accelerated triton beams (10^{8}/s) using the AGOR cyclotron [4]. Worldwide there are presently no accelerator facilities that generate intense triton beams.

With these facts in mind, a list of potential reactions that might be amenable to measurement using ICF was developed. The guiding principles used in selecting these reactions were:

1. The reactions should lead to products that decay with a half-life of more than about 20 ms and less than about 10 s. The decays could then be counted in the quiet environment well after the laser shot, avoiding the difficulty of identifying prompt reaction products.

2. Since in general the cross section will fall as the nuclear charge increases, only target materials up to about Z=7 were considered.

3. The reactions must be energetically allowed at these low energies, so only reactions with a threshold energy of zero were considered.

4. Tritium reactions are preferred, since because there are no accelerators producing triton beams so few previous measurements have been made, even at higher energies.

5. Reactions involving target isotopes with high natural abundance are preferred over those requiring enriched materials.

What could be measured?

For these low-Z nuclei, the tritium reactions that satisfy the no threshold requirement are typically (t,p), (t,γ) and (t,α). Moreover, as can be seen in Figure 1 which shows the chart of nuclides with Z < 8, there are numerous isotopes just below the line of stability that are possibly reachable by triton reactions, having half-lives in the range 20 ms to 10 s.

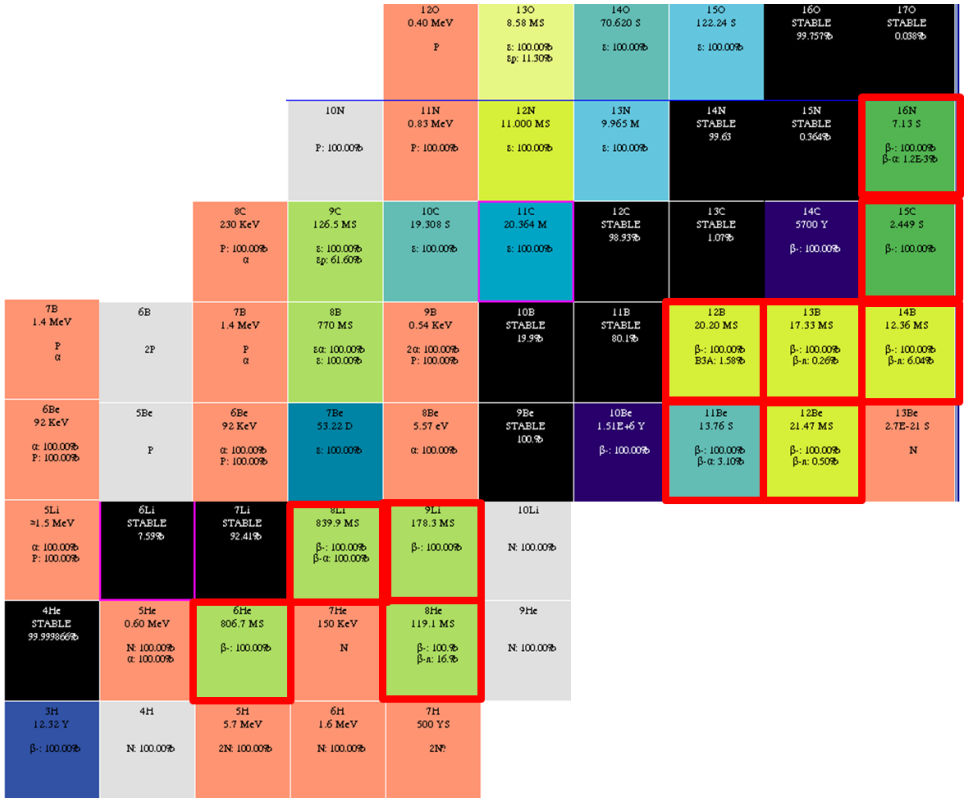

Figure 1. Chart of nuclides [5] for isotopes with Z < 16, with Z increasing vertically and N horizontally. Reactions that might be reached by triton reactions and that have half-lives between about 20 ms and 10 s are outlined with red.

Using the boxed isotopes from Figure 1 as possible reaction products, a list of all possible tritium and deuterium reactions leading to these products was generated. The energy threshold for each reaction was calculated, and those reactions with a threshold of zero were selected for further study, shown in Table 1. Estimates for the total yield and nuclei captured in certain experimental scenarios were then calculated for each reaction.

Table 1. List of candidate reactions currently being studied.

^{3}H(t,γ)^{6}He	^{6}Li(t,p)^{8}Li	^{7}Li(t,α)^{6}He	^{9}Be(t,α)^{8}Li	^{9}Be(t,γ)^{12}B	^{10}B(t,p)^{12}B
^{11}B(d,p)^{12}B	^{13}C(t,γ)^{16}N	^{13}C(t,α)^{12}B	^{13}C(t,p)^{15}C	^{14}N(t,p)^{16}N	^{15}N(d,p)^{16}N

Can the yield be predicted?

The yield for each of the reactions in Table 1 can be estimated by considering the interactions of the nuclei in the reacting plasma. Figure 2 shows a cylindrical volume with circular end area $\mathbf{A}$ containing number density $\mathbf{n_1}$ of ion species 1 traveling with velocity $\mathbf{v}$ through ion species 2 with number density $\mathbf{n_2}$.

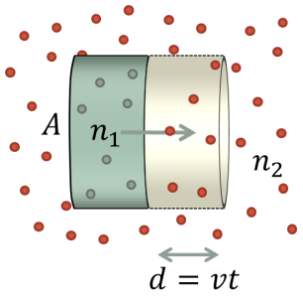

Figure 2. Two ion species interacting in a plasma. A cylindrical volume of ions, $\boldsymbol{V = Ad = Avt}$, containing number density $\boldsymbol{n_1}$ of ion 1 is traveling through a region of space containing number density $\boldsymbol{n_2}$ of ion 2.

In time t each ion 1 travels through distance $d = vt$. The total number of interactions, N, is therefore

$$N = \sigma\ N_1 \frac{N_2}{A} = \sigma(n_1 A\, d)(n_2 d) \tag{1}$$

where σ is the total cross section for the reaction of interest between the two ion species at the incident ion energy $E_1 = \frac{1}{2} m_1 v_1^2$ (assuming non-relativistic energies). The number of ions of each species in the volume $V = Ad$ are N_1 and N_2. The reaction rate, or number of reactions per unit volume per unit time, R, is

$$R = \frac{N}{(Ad)t} = n_1 n_2 \sigma\, v. \tag{2}$$

The above derivation assumed that all of ion species 1 have the same energy, and ion species two is at rest. This is not the case for a high-temperature plasma, however, in which both sets of ions have a thermal velocity distribution at temperature T. In this case, we must use the average reactivity $\langle \sigma v \rangle$ instead,

$$R = n_1 n_2 \langle \sigma v \rangle = f_1 f_2 \left(\frac{\rho}{\bar{m}}\right)^2 \langle \sigma v \rangle_{1,2}. \tag{3}$$

As indicated, the expression for R can also be written in terms of the number fractions $f_1 = n_1/n$ and $f_2 = n_2/n$ where n is the total number density, $n = \rho/\bar{m}$, where ρ is the total mass density and $\bar{m} = (m_1 + m_2)/2$ is the average ion mass. The reactivity, which averages the cross section over the thermal distribution of ion energies, and accounts for the relative motion of the two ion species, is given by

$$\langle \sigma v \rangle = \frac{4}{\sqrt{2\pi m_r (kT)^3}} \int_0^\infty \sigma(E)\ E\, e^{-\frac{E}{kT}}\, dE \tag{4}$$

where $\boldsymbol{m_r}$ is the reduced mass $\boldsymbol{m_r} = \frac{\boldsymbol{m_1 m_2}}{\boldsymbol{m_1 + m_2}}$ and $\boldsymbol{E}$ is the center-of-mass energy. The yield, or total number of reactions in a given volume, is roughly proportional to the reaction rate, assuming the reaction rate is not changing rapidly over the volume and time interval,

$$Y_{1,2} \propto R_{1,2} = f_1 f_2 \left(\frac{\rho}{\overline{m}}\right)^2 \langle \sigma v \rangle_{1,2}, \tag{5}$$

so, assuming the ions are thoroughly mixed and the ratio of the reactivities is roughly constant over the temperature range in the fuel,

$$\frac{Y_{XT}}{Y_{DT}} \cong \frac{f_X f_T}{f_D f_T} \frac{\langle \sigma v \rangle_{XT}}{\langle \sigma v \rangle_{DT}} \tag{6}$$

where D and T represent deuterons and tritons in the fuel, and X is the dopant. Y_{DT} is therefore the number of DT reactions using $\langle \sigma v \rangle_{DT}$, the reactivity for DT reactions at the plasma ion temperature, and Y_{XT} is the number of reactions between the dopant X and the tritons, using reactivity $\langle \sigma v \rangle_{XT}$.

In order to use Equation (6) to estimate the yield that could be obtained for a given reaction under conditions created in an imploding target capsule with the OMEGA laser, estimates for the reactivities $\langle \sigma v \rangle_{XT}$ and $\langle \sigma v \rangle_{DT}$ are needed. The standard formula for the DT reactivity as a function of temperature from Ref. [6] was used and is shown in Figure 3 (f).

How small are the cross sections?

In order to estimate the reactivities as a function of temperature for the reactions in Table 1, estimates for the cross sections for these reactions at low energies were integrated in Equation (4). Of course, the motivation for this research is that these cross sections have never before been measured at these low energies, which means the cross sections used to make the yield estimates must themselves be estimated. This is usually done by either a straightforward extrapolation using a constant S-factor that has been fit to previous measurements at higher energy, or by a more sophisticated theoretical compound nucleus calculation.

In the S-factor formalism the energy dependence of the Coulomb barrier penetration is factored out, leaving a function $S(E)$ that contains the nuclear physics of the specific reaction,

$$\sigma(E) = \frac{S(E)}{E} \exp\left(-\sqrt{\frac{E_G}{E}}\right), \tag{7}$$

where $E_G = (\pi \alpha Z_1 Z_2)^2 2 m_r c^2$ is called the Gamow energy. Far from any resonances, the S-factor function, $S(E)$, is a typically slowly varying function of E that can often be accurately approximated by a constant value or the first few terms in a Taylor series fit to measurements at higher energies, and then used to extrapolate to lower energies. This technique was applied [7] in order to extrapolate to low energies the cross sections for the ^{6}Li(t,p)^{8}Li and ^{7}Li(t,γ)^{6}He reactions from measurements.

Low energy cross sections for these candidate reactions have also been calculated using the code TALYS-1.9 [8], which can produce cross section predictions in the 1 keV – 200 MeV range for nuclear reactions involving neutrons, protons, deuterons, tritons, ^{3}He and alpha particles with targets having $Z \geq 3$ and $A \geq 5$. This code implements a number of nuclear reaction models to predict every possible reaction channel. The optical model is used with a number of different optical model parameterizations and a nuclear structure database to obtain the total cross section and the

elastic and inelastic components as well as other information needed by the other models. A variety of different reaction models are then used to calculate cross sections for specific reaction channels involving direct reaction, pre-equilibum, compound nucleus, and multiple emission processes. At the low energies of interest here, the optical model and compound nucleus models are the most significant, but they all play a role in accurately determining how the cross section is partitioned between the competing reaction channels.

Neither of these techniques can be used to predict the cross section for the ^{3}H(t,γ)^{6}He reaction however. It has never been measured before at any energy so an S-factor extrapolation is impossible, and the target has $A < 5$ which is not allowed by TALYS. Attempts are being made to use the code AZURE2 to calculate this cross section. AZURE2 uses the R-matrix formalism to describe different reactions in the same compound system simultaneously with a single set of parameters. This will allow other reactions that pass through the ^{6}He compound nucleus to be used to fit the parameters needed to calculate the ^{3}H(t,γ)^{6}He cross section. R-matrix calculations have previously been made for the ^{6}He compound nucleus in order to calculate ^{3}H(t,2n)^{4}He cross sections [9] that may be useful here.

Cross section predictions made using TALYS and S-factor extrapolations for the reactions listed in Table 1 are plotted in Figure 3, along with all the known measurements at energies less than 1 MeV. As expected from the Coulomb repulsion, the largest cross sections are for the ^{6}Li(t,p)^{8}Li and ^{7}Li(t,α_0)^{6}He reactions in Figure 3 (a). In Ref. [7] the ^{6}Li(t,p)^{8}Li cross sections from Ref. [10] were normalized to 20 mb at 1 MeV, and the S-factor fit at low energies. It is not surprising the S-factor extrapolation agrees well, therefore, since it was based on a fit to these data, while the TALYS predictions are about a factor of two larger. Because the first exited state of ^{6}He decays by two-neutron emission, the calculations for ^{7}Li(t,α_0)^{6}He are for the channel leaving the ^{6}He in its ground state, the excitation function for which was estimated by multiplying the excitation function to the first excited state by 1/10, a factor approximately constant for energies less than about 300 keV [11].

Cross sections predicted by TALYS for the other reactions are shown in Figure 3 (b) – (e). In every case where measurements have been made at higher energies, the measured cross sections are higher than the TALYS prediction, by a factor of 2 in the case of ^{9}Be(t,α)^{8}Li to as much as a factor of 100 for ^{15}N(d,p)^{16}N. In general, predicted (t,α) cross sections are about 10 times the (d,p) and (t,p) cross sections, which are very similar above about 500 keV. The (t,γ) cross sections are approximately 10^{-4} times smaller than the (t,p) cross sections.

Figure 3 (f) shows the reactivity as a function of ion temperature, determined by integrating Equation (4) for each of the predicted cross sections. For comparison, the total reactivity for DT fusion and ^{3}H(t,2n)^{4}He are also shown. It might be expected that the "best case" branching ratio for ^{3}H(t,γ)^{6}He might be 10^{-5}. This is also plotted so that it may be compared with the reactivities for the other reactions of interest. Several complicating factors, however, make it unlikely the reactivity is this high.

Table 3 lists all of the reactions, giving the half-life of the reaction product and the natural abundance of the dopant, along with estimated yields based on the parameters for two typical OMEGA shots, having parameters shown in Table 2. OMEGA shot 39794 was a DT shot using a 2.8 μm thick SiO_2 capsule filled with 20 atm of deuterium-tritium mix reaching an ion temperature of 11.8 keV, whereas shot 77951 was a tritium-filled SiO_2 capsule "exploding pusher" reaching 18.3 keV. Also shown is the expected number of product nuclei that might be collected, based on the solid angle in a particular detection scheme, described later.

As expected, the yield tends to fall as the charge of the dopant nucleus increases. The orange highlighted reactions, ^{3}H(t,γ)^{6}He, ^{6}Li(t,p)^{8}Li, ^{7}Li(t,α)^{6}He, and ^{9}Be(t,α)^{8}Li, are the ones predicted to have large enough yields that a measurement may be possible. The green highlighted reactions, ^{10}B(t,p)^{12}B and ^{11}B(d,p)^{12}B, may be measureable if the

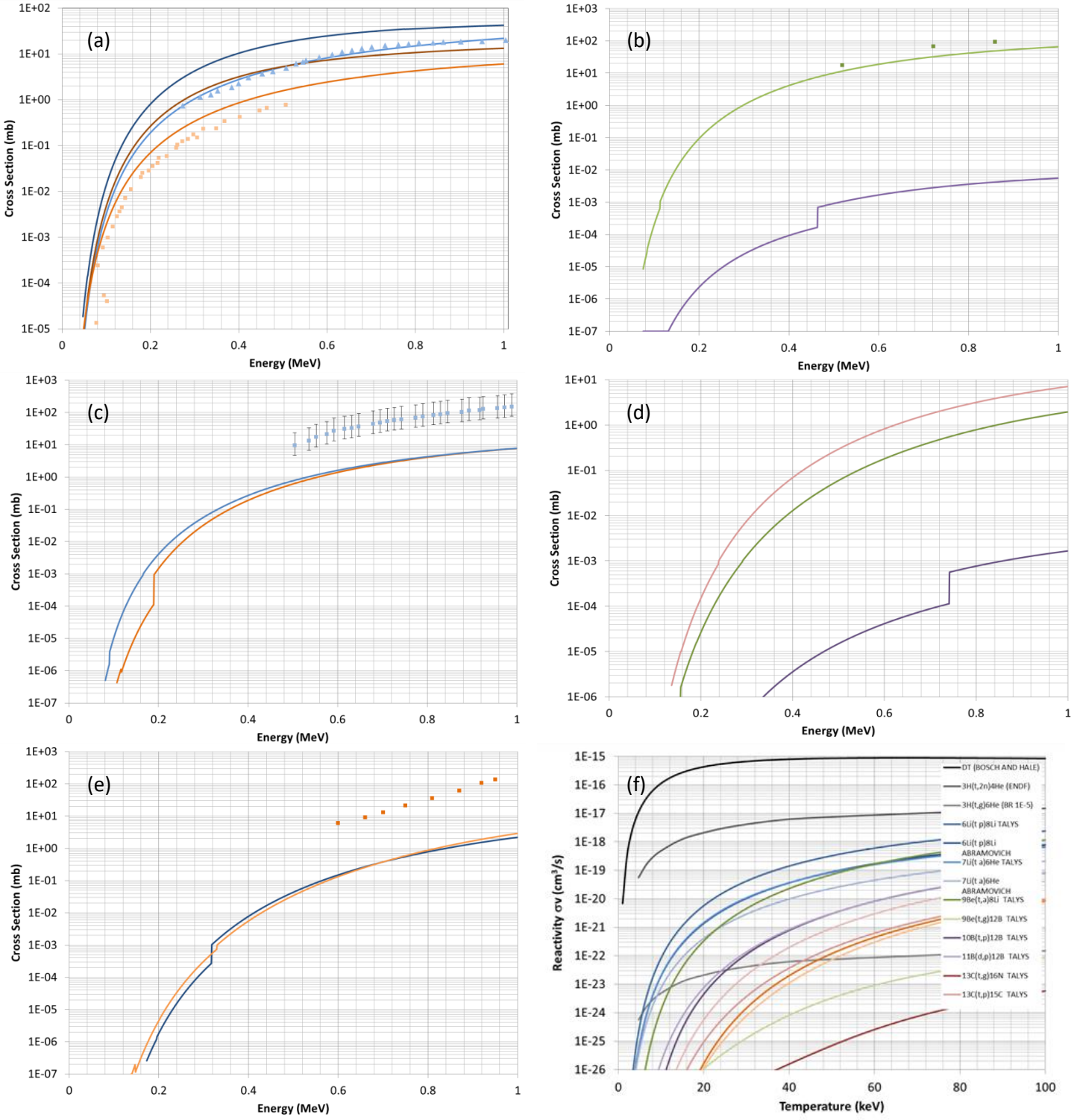

Figure 3. **(a)** Cross sections for ^{6}Li(t,p)^{8}Li predicted by TALYS (dark blue curve), S-factor [7] (light blue curve) and measured [12] (light blue triangles), and for ^{7}Li(t,α_0)^{6}He predicted by TALYS (dark brown curve), S-factor [7] (orange curve) and measured [10, 11] (orange squares). **(b)** Cross sections for ^{9}Be(t,α)^{8}Li predicted by TALYS (green curve), and measured [13] (green squares), and for ^{9}Be(t,γ)^{12}B predicted by TALYS (purple curve). **(c)** Cross sections for ^{10}B(t,p)^{12}B predicted by TALYS (orange curve), and for ^{11}B(d,p)^{12}B predicted by TALYS (blue curve) and measured [14] (blue squares). **(d)** Cross sections for ^{13}C(t,p)^{15}C (green), ^{13}C(t,γ)^{16}N (purple) and ^{13}C(t,α)^{12}B (pink) predicted by TALYS. **(e)** Cross sections for ^{14}N(t,p)^{16}N predicted by TALYS (blue curve), and for ^{15}N(d,p)^{16}N predicted by TALYS (orange curve) and measured [15] (orange squares). **(f)** Reactivities calculated by integrating Equation (4) for each of the predicted cross sections.

Table 2. Parameters for OMEGA shots 39794 and 77951 used in Equation (6) to calculate the yields in Table 3.

	Shot 39794	**Shot 77951**
DT Yield	3.8×10^{13}	2.6×10^{11}
f_D	56%	1.5%
f_T	39%	98.5%
kT	11.8 keV	18.3 keV
Dopant	1%	1%

Table 3. List of reactions meeting the criteria for measuring via ICF using the OMEGA laser, showing halflife and abundances of the reactant isotopes. Estimated yields and detector counts are given for two typical OMEGA shots. Candidate reactions for an experiment are highlighted orange.

Reaction	Product Half-life	Reactant Abund.	Shot 39794 (50-50 DT, 11.8 keV) Predicted Yield	Shot 39794 Captured	Shot 77951 (1.5-98.5 DT, 18.3 keV) Predicted Yield	Shot 77951 Captured	Notes
$^{3}H(t,\gamma)^{6}He$	807 ms	^{3}H fill	Branching ratio of ~10^{-7} to $^{3}H(t,2n)^{4}He$ gives		8×10^{4}	200	To ^{6}He g.s. only, excited states decay by 2n
$^{6}Li(t,p)^{8}Li$	840 ms	7.6%	$2\text{-}10\times10^{5}$	1000-6000	$4\text{-}16\times10^{5}$	2000-9000	TALYS + Abramovich et. al.
$^{7}Li(t,\alpha)^{6}He$	807 ms	92.4%	$1\text{-}3\times10^{5}$	500-1500	$1\text{-}4\times10^{5}$	700-2300	TALYS + Abramovich et. al. To ^{6}He g.s. only, excited states decay by 2n
$^{9}Be(t,\alpha)^{8}Li$	840 ms	100%	2.3×10^{4}	130	8×10^{4}	460	TALYS
$^{9}Be(t,\gamma)^{12}B$	20.2 ms	100%	2.8	0.02	3.0	0.02	TALYS
$^{10}B(t,p)^{12}B$	20.2 ms	19.9%	78.3	0.44	923	5.2	TALYS
$^{11}B(d,p)^{12}B$	20.2 ms	80.1%	372	2.09	1735	9.8	TALYS
$^{13}C(t,\gamma)^{16}N$	7.1 s	1.1%	0.05	0.0003	0.1	0.001	TALYS
$^{13}C(t,\alpha)^{12}B$	20.2 ms	1.1%	8.2	0.05	108	0.6	TALYS
$^{13}C(t,p)^{15}C$	2.45 s	1.1%	1.2	0.01	17.7	0.10	TALYS
$^{14}N(t,p)^{16}N$	7.1 s	99.6%	0.06	0.0003	2.5	0.01	TALYS
$^{15}N(d,p)^{16}N$	7.1 s	0.4%	0.10	0.0006	2.0	0.01	TALYS

cross section is higher than the TALYS prediction, which is likely as indicated by the disagreement with experiment at higher energies. The $^{3}H(t,\gamma)^{6}He$ reaction is likely to be measureable, but since it has never been measured before an R-matrix calculation is needed.

How would it work?

After the ICF implosion, the product nuclei will initially be ions in the plasma that will lose energy very quickly as they travel through the plasma. Since they have a relatively large charge, they will not have enough energy to escape from the plasma, and will eventually thermalize and recombine to form neutral atoms. In order to count the number of product nuclei then, a means must be found to collect and trap the neutral atoms, and count their nuclear decays.

Non-reactive product gases, such as ^{6}He or possibly ^{16}N, would not stick to most surfaces, and would need to be mechanically or thermally trapped, whereas some of the other products could possibly stick to a getter or even the walls of a mechanical system. Three techniques are being considered, shown in Figure 4.

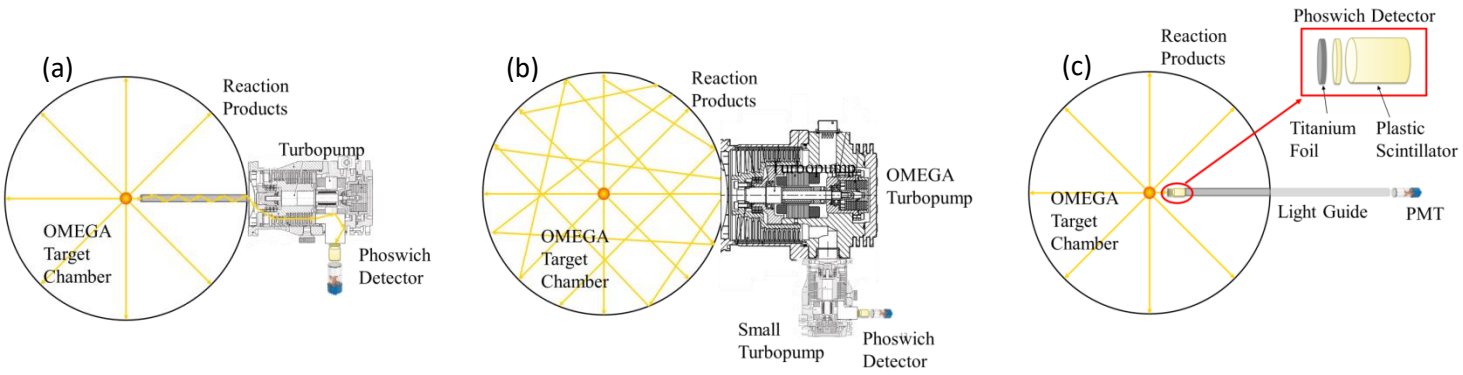

Figure 4. Three methods for collecting the neutral radioactive product atoms. (a) Atoms enter a long tube near the target chamber center, are trapped by a turbopump, and their decays counted in the sealed turbopump exit port. (b) A large turbopump simply evacuates the target chamber after the shot, and the decays are counted in the sealed exit port. (c) Reaction products stick to a getter material that is in front of the detector, near the target chamber center.

a) A long gas collection tube could be extended very near to the target chamber center (TCC). Gas molecules from the target would travel freely down the evacuated tube, where they would be trapped by a turbopump in a sealed tube attached to the exit port and counted. Even at room temperature, the gas molecules would only take about 1.5 ms to reach the detector. Assuming the gas is expanding isotropically this method has the advantage that the fraction of the gas collected can be calculated from the solid angle, since all the rest of the gas in the chamber will have a very high probably of being removed by the large cryopumps and will never enter the small tube. The maximum size of the tube without interfering with the lasers was estimated to be about the same as the Neutron Temporal Diagnostic [1], with a tube radius of 3 mm located 2 cm from the TCC. This solid angle was used to determine the "collected" columns in Table 3.

b) A large turbopump could be mounted to the target chamber, and simply used to collect all the gas similar to the Omega Gas Sampling System (OGSS) [16]. This method would have the advantage of collecting all of the product nuclei, assuming they did not stick to the chamber wall. However, assuming a pump entrance radius of 15 cm (same as an OMEGA cryopump) and modeling the process as effusion through the orifice into a perfect vacuum, gives the estimate that it would take about 16 s to remove all the gas from the chamber if it starts at 10^{-5} torr, and 1 s to remove 20 %. This is an underestimate since there is not a perfect vacuum inside the cryopump, and in fact the OGSS reported it took 90 seconds to remove the gas with the cryopump. This means this method probably would not work except for the longer-lived products, such as ^{16}N.

c) For products that are not inert gases, a getter foil could be attached to the face of the plastic scintillator detector, and this assembly placed very close to the TCC. Ions from the implosion would hit the getter first, ablating and

cleaning the surface, followed by neutral atoms which could stick and be counted. A long light guide would allow the PMT to be far away.

Can these ideas be tested?

In order to test the feasibility of these ideas and to answer the questions that naturally will arise, an experimental testbed is being developed to simulate the environment of the OMEGA target chamber, and allow the fast release of various stable and radioactive gases and the fast measurement of pressure changes. The basic system, shown in Figure 5, has several components that can be used to carry out a variety of experiments.

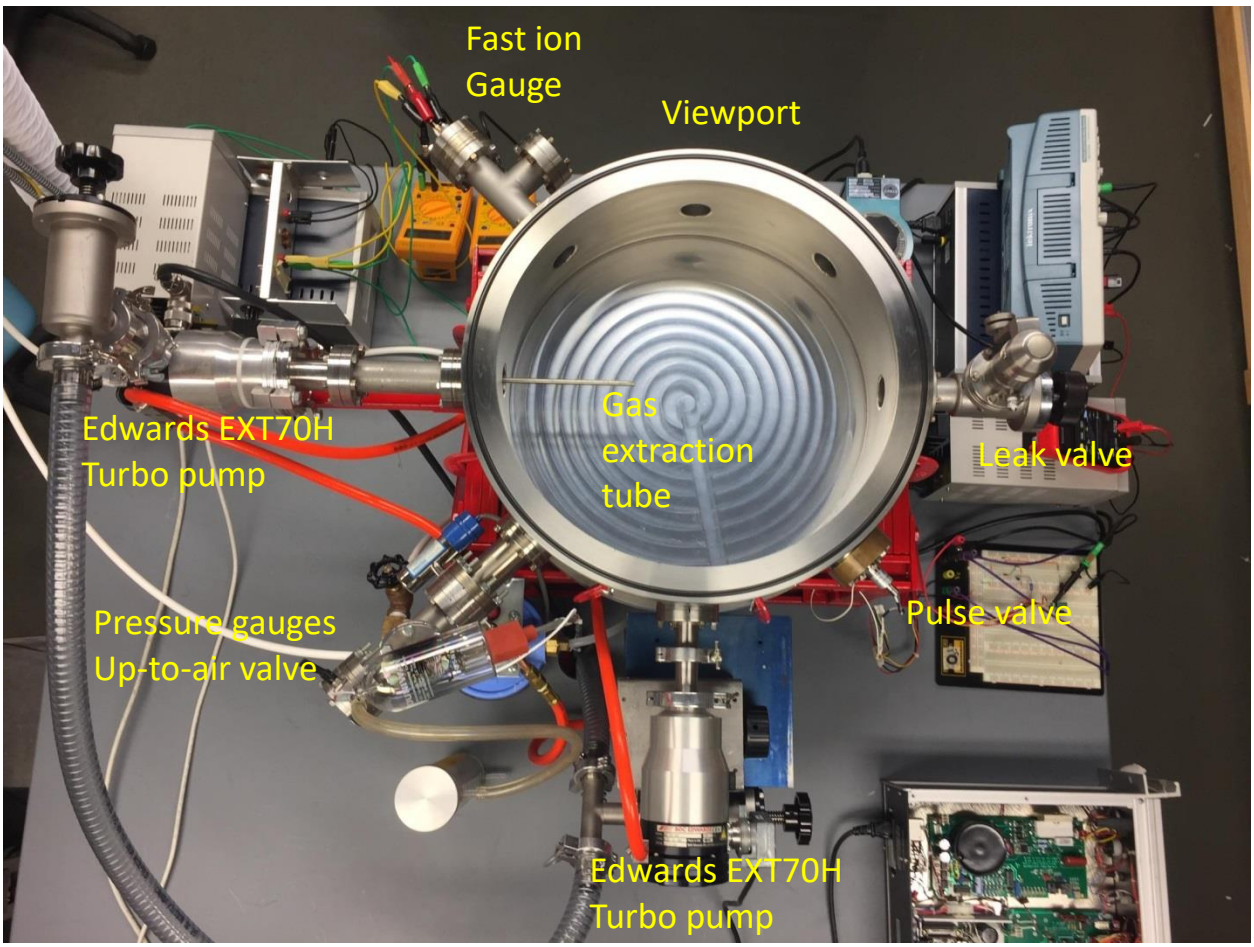

Figure 5. The experimental test system. The gas extraction tube leads to one of the turbopumps, which traps the atoms in its sealed exit port. A second turbopump evacuates the chamber. The fast valve can allow gas pulses as short as a few hundred microseconds to enter the chamber, where they can be measured by the fast ion gauge. A commercial ion gauge, thermocouple gauge, and leak valve are used for calibration and monitoring.

1. Vacuum system

The 50.8 cm (20 in.) diameter, 15.24 cm (6 in.) high stainless steel vacuum chamber has eight 2.75 in. conflat ports around its perimeter. The top and bottom lids are 1.27 cm (0.5 in.) thick aluminum that seal to the chamber with rubber o-rings in grooves in the top and bottom chamber flanges. A new top lid (see Figure 6) has been ordered that will have two 2.75 and three 1.33 in, conflat ports for inserting ionization gauges and targets.

The chamber is evacuated by a water-cooled Pfeiffer TPH062 Turbomolecular pump backed by an Alcatel Pascal 2005 SD rotary forepump. Attached to the chamber are two pressure gauges, a Duniway T-075-N ionization gauge with a Varian Multigauge controller and a Granville-Phillips convectron convection gauge with a GP 275 controller. A Varian 951-5100 variable leak valve allows the pressure in the chamber to be controlled and the gauges to be cross calibrated. A Parker Precision Fluidics 009-0181-900 Ultra Low Leak Extreme Performance Valve allows extremely short bursts of gas into the chamber. A homemade fast ion gauge is attached, and a viewport. The 0.635 cm (0.25 in.) stainless steel gas extraction tube allows gas to travel to a second water-cooled Edwards EXT70H Turbo pump where it can be trapped and compressed by valving off the foreline.

2. Fast Ionization Gauge

A number of tiny fast ionization gauges, shown in Figure 6 , have been constructed following the description given by T. E. Weber, and T. P. Intrator [17]. According to their paper, these gauges, which will operate over the pressure range of $< 10^{-6}$ Torr to 300 mTorr, can have leading edge rise times as fast as 200 μs and can measure pressure change rates of at least dp/dt ≈ 375 Torr/s .

Figure 6. (Left) The high speed ionization gauge. The filament is the smaller winding, the grid is the larger winding which is coaxial with the collector wire. (Center) Houghton student Emma Bruce needs steady hands to carefully clip the leads on the ion gauge she has just completed. (Right) A new vacuum chamber lid will have ports for inserting these ion gauges, as well as gas sources, to measure the motion of gas in the chamber.

A new vacuum chamber lid, shown in Figure 6, was ordered on May 8, 2018. When it arrives, it should be possible to measure the changes in the pressure across the vacuum chamber on the 100 μs time scale. By placing ion gauges in the ports along a line leading away from the fast valve at the edge of the chamber, the progress of the gas across the chamber could be measured, while having the gauges along a line perpendicular to the motion of the gas would allow the evolution of the gas density profile to be measured. For gas sources at the center of the chamber, such as various laser targets , these gauges could be placed at different angles and used to measure the isotropy of the expansion.

The ion gauge readout circuit is shown in Figure 7. A current through the filament of about 1 A is sufficient for the thermionic release of electrons which are attracted by the approximately +100 V potential on the grid. Traveling past the grid, they can ionize the gas, with the ions being collected on the grounded collector wire. Both the collector and emission currents can be measured as a voltage drop when these currents flow through 100 kΩ and 100 Ω resistors, respectively. The original paper specified a 1 kΩ resistor rather than a 100 kΩ resistor, which we found was needed to get adequate voltages to measure with an oscilloscope. This may be why our gauge seems slower than the one described in the paper.

In order to test and calibrate the gauges, they are taken to a separate vacuum chamber where the pressure is allowed to rise slowly, and the emission and collection currents are measured as a function of the pressure recorded by another ion gauge. As shown in Figure 7 the response is very linear over the range of $\sim 5 \times 10^{6}$ to 3×10^{-4} Torr.

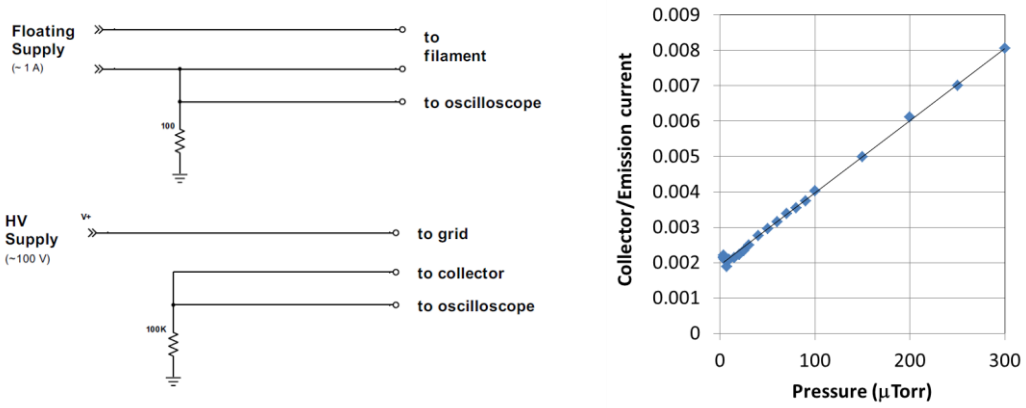

Figure 7. (Left) The circuit used to read out the fast ion gauge. (Right) A typical fast ionization gauge calibration curve for air, measured by slowing allowing the pressure in the chamber to rise.

3. Fast Valve

A Parker Precision Fluidics 009-0181-900 Ultra Low Leak Extreme Performance Valve is attached to the chamber to allow fast pulses of gas to enter. It is a poppet-type valve with a solenoid that very quickly lifts the poppet and a spring that returns the poppet, closing the valve. Normal operation of the valve requires an initial voltage of around 200 V for several hundred microseconds, followed by a 28 V holding voltage. Nominally, the shortest achievable pulse duration is 300 μs, the opening response time is 180-200 μs and the closing response time is 50-250 μs. Up to 600 V in a short duration pulse has been applied to further increase the opening speed [17].

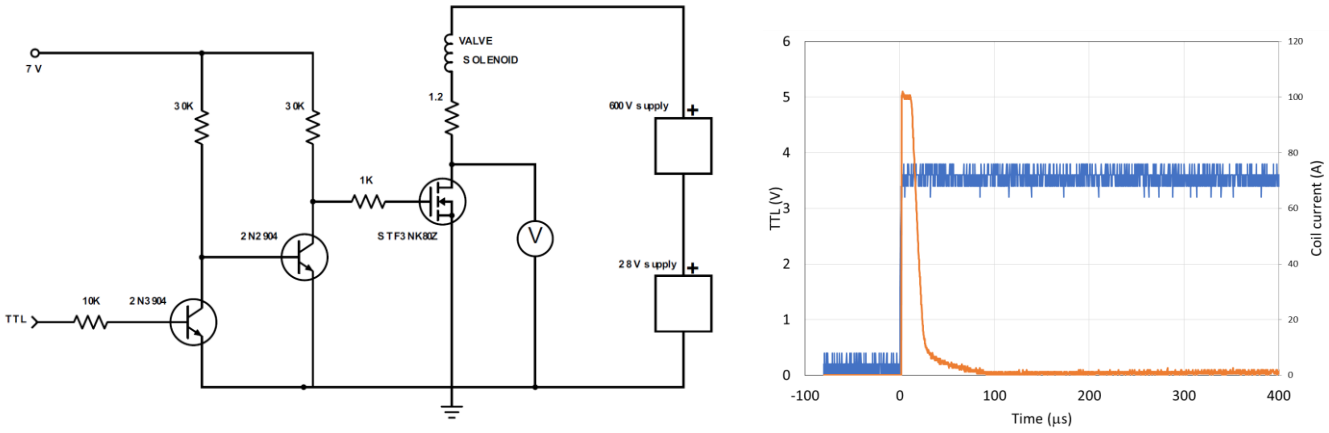

Figure 8. (Left) Circuit diagram for the fast valve driver circuit. (Right) The leading edge of the TTL trigger pulse (blue) and the current flowing through the valve coil (orange). When the circuit was triggered, in this example about 150 V was placed across the coil, resulting in a current of about 100 A that lasted for about 30 μs, opening the valve quickly. After that the voltage fell to about 30 V with a current of about 0.5 A to hold the valve open.

The circuit shown in Figure 8 was designed to apply the needed voltage time structure. An Arduino microcontroller produces a TTL pulse of controlled duration which turns on a MOSFET allowing current to flow through the valve

solenoid coil. The bipolar transistors are needed to produce a non-inverted pulse of adequate voltage to turn on the MOSFET. The measured voltage across the 1.2 Ω resistor allows the current through the solenoid to be determined.

The current through the solenoid is also shown in in Figure 8. When the MOSFET is first turned on, the full voltage across both power supplies is across the solenoid, about 150 V in this case, resulting about 100 A of current. This current very quickly pulls down the voltage across the HV power supply; after about 30 μs the current falls to about 0.5 A, maintained by the 28 V power supply, which keeps the valve open. The duration of the HV pulse can be increased by adding storage capacitance across the terminals of the HV power supply.

The rms velocity of N_2 molecules in air is about 500 m/s. The time required for air to cross from the fast valve to the fast ion gauge can therefore be calculated to be about 1.2 ms. This transit time was measured and the results are shown Figure 9. The pressure begins to rise about 1.2 ms after the solenoid is energized. Unfortunately the rise time is about 8 ms, which his much longer than the expected 200 μs, possibly because the valve was only pulsed with 150 V or because of the high resistance readout resistor attached to the collector.

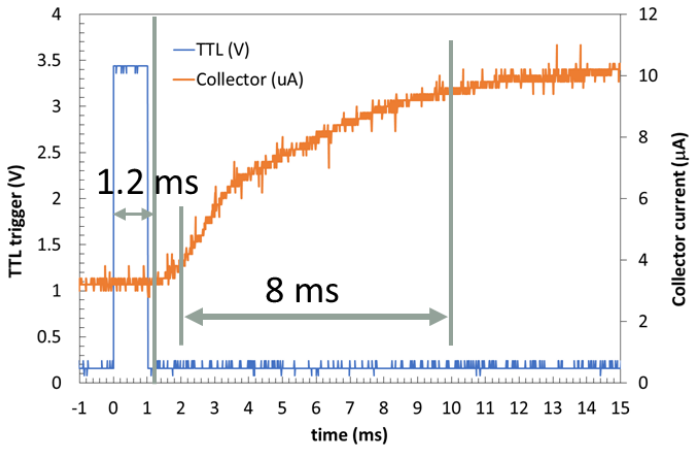

Figure 9. The result of the fast valve and fast ion gauge test. The TTL trigger was used to open the fast valve, which allowed a puff of air to enter the evacuated vacuum chamber. The approximate time required for N_2 to cross the chamber, based on its rms speed at room temperature, should be about 1.2 ms. The measured 8 ms rise time is much longer than the expected 200 μs.

4. Laser System

A 6 W 445 nm Nichia NUBM 44 laser diode can be used, by entering through a vacuum window, to vaporize target cells, microballoons, and various surfaces for the purpose of producing bursts of radioactive and stable gases inside the vacuum chamber. The laser diode, shown in Figure 10, is housed inside a heat sink, and powered by a driver circuit in a separate aluminum box that also houses an Arduino microcontroller. The Arduino is used to produce laser pulses of precise time duration. The laser power may be adjusted by controlling the current drawn from the external power supply.

Hollow microballoons of glass, acrylic and phenolic resin with diameters between about 10 μm and 80 μm are shown in Figure 11 and can be purchased commercially since they are used as a lightweight epoxy filler. Approximately 4 W of laser power was used for a period of a few seconds to see if these microballoons could be "popped". No effect could be seen on the glass or acrylic microballoons, although an ink line on the microscope slide behind them was scorched. Apparently they are so transparent they did not absorb very much laser power. The phenolic microballoons are opaque, but unfortunately phenolic resins are used commercially for their fire-resistant properties. They have no melting point,

and do not decompose until temperatures over about 500 °C, and this only results in charring. Figure 11 shows before and after photographs of charred phenolic microballoons. Currently the possibility of dying acrylic microballoons black is being explored in an attempt to get them to absorb enough laser power to melt, since the melting point of acrylic is only about 130 °C.

Figure 10. (Left) The 6 W 445 nm Nichia NUMB 44 laser diode is encased in a large heat sink, and powered by the laser driver power supply inside the aluminum enclosure, which also contains the Arduino that provides the timing signal used to produce precise duration laser pulses. (Center) The NUMB 44 laser in action, the beam hitting the laser power meter. (Right) Houghton student Sarah Hull using the microscope to examine the results of hitting the microballoons with the laser.

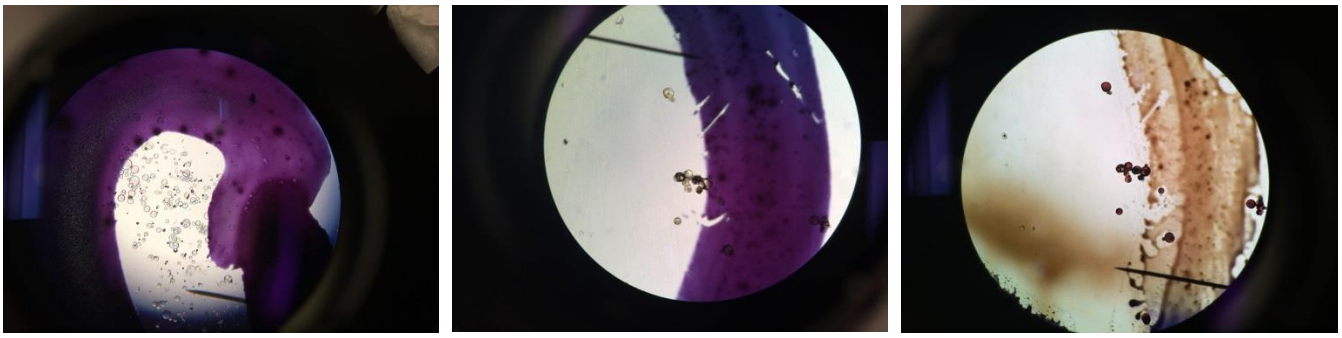

Figure 11. (Left) Acrylic microballoons (about 10 μm to 80 μm in diameter) at 100x. The purple color is a tiny circle drawn on the microscope slide with permanent ink. (Center) Phenolic microballoons before being exposed to laser power. (Right) Same phenolic microballoons after being hit with the laser. The microballoons look "charred" and the purple ink has been scorched.

5. Phoswich Detector

Over the past two summers a phoswich detector system for detecting beta particles from short half-life radioisotopes was developed, and is described in the 2017 report. However, the experimental test of this system did not occur until after the report was submitted.

The detector, shown in Figure 12, consists of a thin plastic scintillator (dE) having a short decay time optically coupled to a thick plastic scintillator (E) having a long decay time. Charged particles entering the detector deposit some energy in the thin dE scintillator, and then stop, depositing all of their remaining energy in the thick E scintillator. Different particle species of the same total energy will deposit different amounts in the thin dE scintillator, therefore particles can be identified by where they fall on a 2D histogram of energy deposited in each detector. Light from both scintillators is converted to a current pulse by the photomultiplier tube. An electronic circuit is used to split the fast component from the thin scintillator, which comes in the first few nanoseconds, from the slow pulse from the thick scintillator.

Figure 12 also shows the setup of the experiment that was used to test the phoswich detector's ability to detect ^{6}He, one of the product nuclei from Table 3 with a half-life of 807 ms. An approximately 100 nA beam of 2.0 MeV deuterons from the SUNY Geneseo Pelletron was allowed to strike a 0.36 mm thick deuterated polyethylene sheet that was attached to the rear window of the target chamber. Neutrons produced by the by ^{2}H(d,n)^{3}H reaction then penetrated the vacuum window and interacted with a 19.5 mm by 26 mm by 6.5 mm thick rectangular plate of ^{9}Be where they produced ^{6}He via ^{9}Be(n,α)^{6}He. The ^{6}He nuclei, embedded in the ^{9}Be, beta decayed and the beta particles were detected by the phoswich detector.

Figure 13 shows the 2D histogram that was obtained by plotting the energy deposited in the dE detector versus in the E detector. Events in the clearly defined electron band in the histogram were counted, and the resulting decay curve plotted as a function of time. The measured half-life was 789.2 ± 37.8 ms, which agrees with the accepted value of 807 ms.

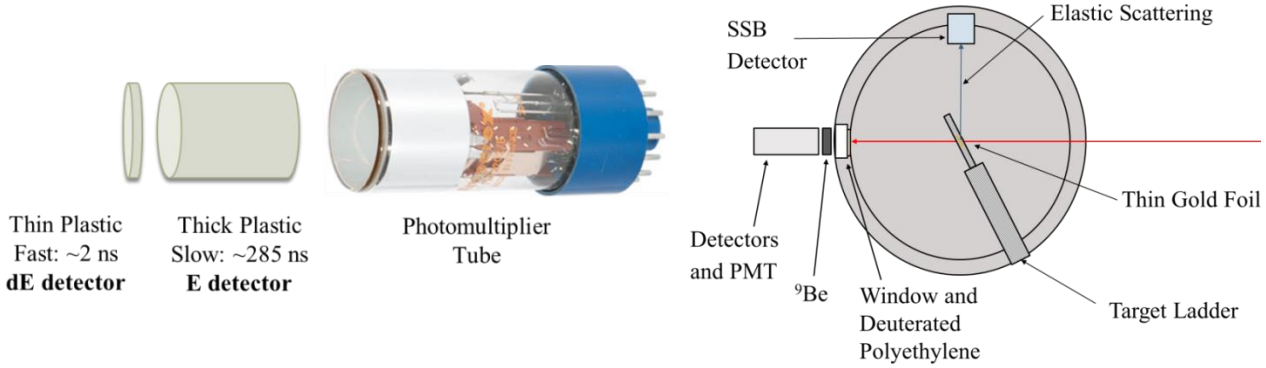

Figure 12. (Left) The phoswich detector consists of a thin plastic scintillator with a short decay constant optically coupled to a thick plastic scintillator with a long decay constant, which is coupled to a photomultiplier. (Right) The experimental setup at SUNY Geneseo for testing the phoswich detector. Deuterons strike a deuterated polyethylene film producing neutrons which then create ^{6}He in a ^{9}Be target via ^{9}Be(d,α)^{6}He.

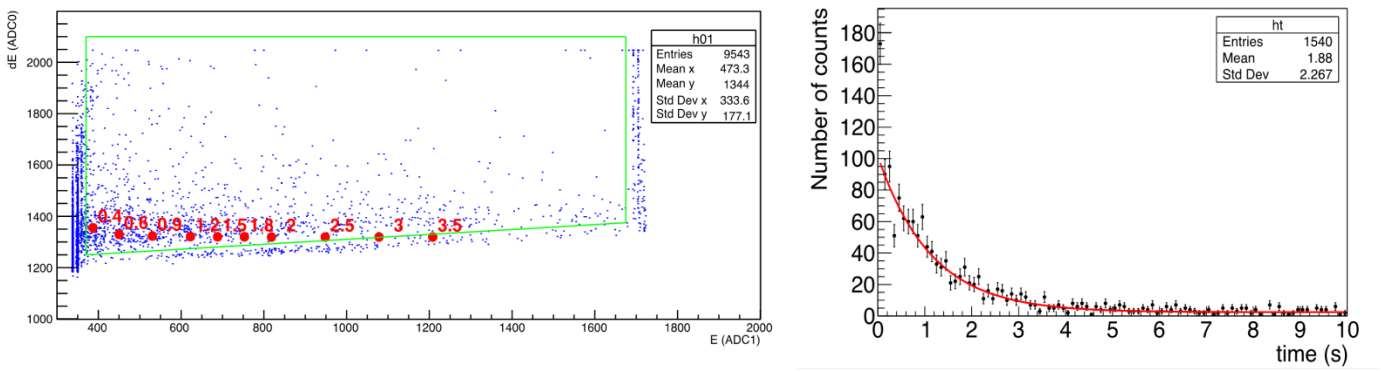

Figure 13. (Left) A 2D histogram of energy deposited in the thin scintillator (dE) vs. the thick scintillator (E). The red dots indicate the approximate expected location of electrons of the indicated energy in MeV. The green polygon includes the events that were counted as electrons. (Right) The number beta decay events (events inside the green polygon) as a function of time.

What experiments can be done with this test system?

Many questions need to be answered before a measurement of this type could be made. The first experiment, which is currently underway, is to see if we can create, release, trap with a turbopump, and detect the decay of an inert radioactive gas. Following a description of this experiment, a list of possible future experiments will be given.

1. ^{40}Ar(d,p)^{41}Ar Experiment

The isotope ^{41}Ar is an inert gas that will behaves like ^{6}He in many ways – it does not react chemically and it beta decays with an endpoint energy of 1.2 MeV -- but it has the advantage of a much longer half-life than ^{6}He, 109 min as opposed to 807 ms. This allows for the isotope to be produced at SUNY Geneseo and transported to Houghton College, travel time 45 minutes, where it can be inserted into the test system. If a technique can be developed that will allow ^{41}Ar to be captured, trapped and detected there is a very good chance it will also work for ^{6}He, which is one of the products in Table 3.

The ^{41}Ar can be created using the reaction ^{40}Ar(d,p)^{41}Ar, which has a cross section of about 0.2 b at 3 MeV. Deuterons of this energy were accelerated using the SUNY Geneseo Pelletron and allowed to penetrate an 18 μm thick kapton window located at the far side of the end chamber. The deuterons then entered an argon-filled gas cell.

The PVC gas cell, shown in Figure 14, has an aluminum cap that fits snugly around the kapton window flange with a rubber O-ring. A copper fill tube enters this cap, and allows the cell to be filled with 1 atm of natural argon, ^{40}Ar. The gas cell itself consists of two PVC valves and an end-cap. When filling the cell both valves are opened and the end cap is removed to flush the cell out as much as possible. Then the back PVC valve and the fill line valve are closed and the first PVC valve left open.

After activation for 50 min, the gas cell valves are closed and the cell is removed to a counting station where it was placed next to a high purity germanium detector (HPGe) inside a lead shield. Figure 14 shows the energy spectrum obtained after 4.5 hours of counting. The decay curve was also plotted, and half-life measured to be 110 min, in agreement with the previous measurement of 109.34 min. In total we estimate that 15 million ^{41}Ar were made in 50 minutes of irradiation in our argon gas target.

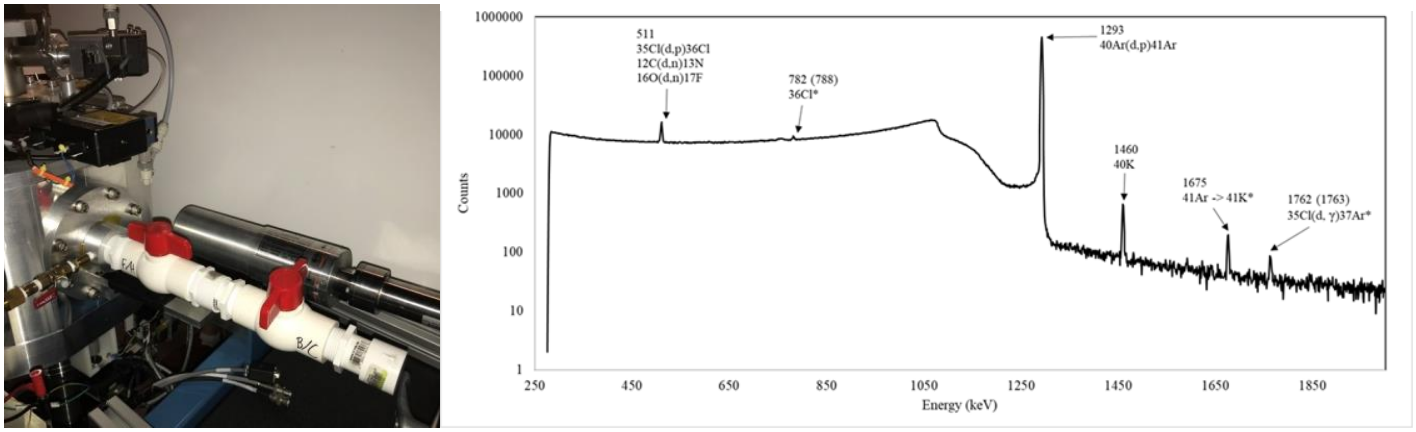

Figure 14. (Left) The argon gas cell attached to the SUNY Geneseo Pelletron target chamber. Deuterons entered through a thin window into a cell filled with ^{40}Ar. (Right) Gamma ray spectrum obtained after the gas cell was removed and counted with an HPGe detector. The 1293 keV gamma ray line from ^{41}Ar was very prominent, and decayed with the half-life of 109 min.

The next step is to create ^{41}Ar and bring it to Houghton College. When the gas cell is ready to be removed from the accelerator end station, the PVC valve is closed trapping the argon and an aluminum stopper is placed into the

aluminum cap, sealing against the rubber O-ring. Once at Houghton, the fill tube is attached to the fast valve, and a forepump is used to remove the air from the fill tube and the aluminum end cap. The PVC valve is then opened, allowing the argon to fill the aluminum cap and the fill line before opening the fast valve to allow it to enter the vacuum chamber. Following this process, with argon at about 1 atm in the cell, opening the fast valve for 800 ms fills the foreline trap to about 500-600 mTorr, which is a significant fraction of the maximum allowed backpressure for the turbopump, 900 mTorr.

For this experiment, the gas extraction tube was extended so that the tube ends about 8 cm from the fast valve outlet. As shown in Figure 15, a valve that can be closed once all of the gas has been collected was placed between the turbopump exit port and the QF16 cross that is used to hold the collected gas. One arm of the cross leads to the foreline, which also can be valved off, and the opposite arm to a Lesker KJC 275 thermocouple gauge for monitoring the pressure in the trap. The top arm of the cross is sealed by a thin kapton window which allows beta particles emitted by the trapped gas to pass into a lithium-drifted silicon detector (Canberra LEC 500-3000) 3 mm thick with an active area of 500 mm^2. A light-tight holder that has a thin aluminum foil entrance window was 3D printed for this detector so that the detector can operate in ambient light. Pressed up as close as possible to the face of the cross was an ORTEC HPGe detector. Singles events from each detector, as well as coincidences between the detectors are recorded using a FAST MPA-4 acquisition system, and, as a backup, each detector also has its singles spectrum recorded by a Spectrum Techniques UCX-30 multichannel analyzer and the silicon decay curve is recorded by an AMPTEK MCA-8000 operating in multichannel scaler mode.

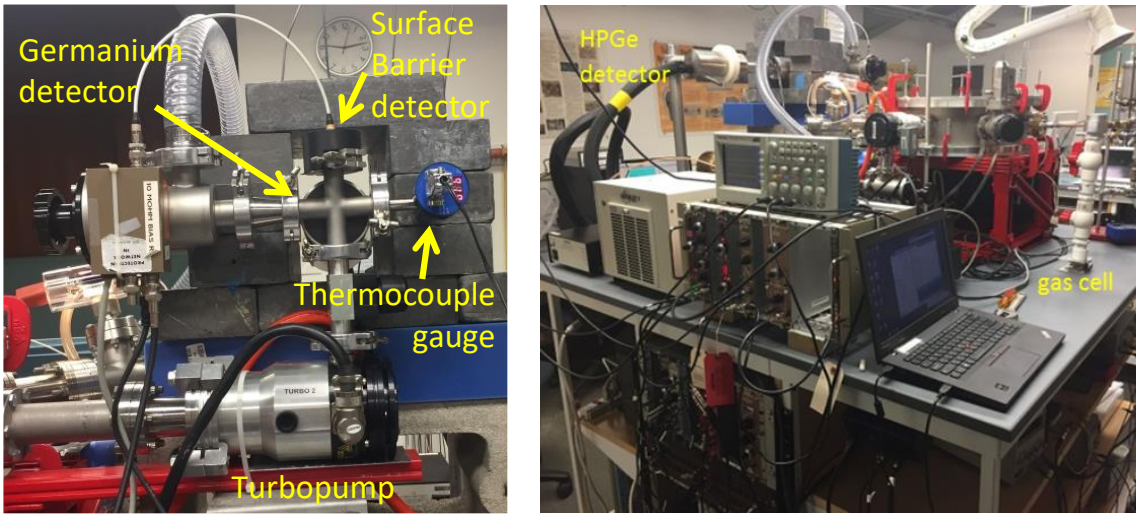

Figure 15. (Left) A mixture of ^{41}Ar atoms and residual gasses from the vacuum chamber leave the turbopump exit port and are trapped in the foreline, which is sealed off. The pressure is monitored with a thermocouple gauge, the beta decays are counted with a silicon surface barrier detector, and the gamma rays with a germanium detector. (Right) The other side of the vacuum chamber, showing the placement of the gas cell and the HPGe detector.

The first attempt to bring ^{41}Ar to Houghton College failed because the kapton window on the accelerator end station ruptured, and almost all of the ^{41}Ar in the gas cell escaped in the vacuum system. The residual gas remaining in the cell was injected into the vacuum system at Houghton, but no decays were counted in the foreline trap of the turbopump by either detector. A second attempt is planned for July 23, 2018.

Figure 16. (Left) Houghton and SUNY Geneseo students working together on the test experiment. (Right) Houghton Student Katelyn Cook used a 3D printer to make a light tight housing for the silicon detector, and is shown here installing the thin foil window that allows the beta particles to enter the detector.

2. Future Experiments

Many other experiments may be performed with this system now that it is assembled, as illustrated in Figure 17. Most of the experiments involve using either the laser or the fast valve to quickly release either a radioactive or stable gas into the system, the turbopump or a getter to collect it, and, if appropriate, a detector to count the decays. These experiments are necessary to understand the behavior of the gas and the capabilities of the trap and detection system in order to have confidence that an experiment using OMEGA will be able to determine the number of product nuclei and thereby measure the reactivity. The most important reaction products to understand are ^{6}He, ^{8}Li, ^{12}B since these result from the reactions with the highest predicted yield, highlighted in orange or green in Table 3, namely ^{3}H(t,γ)^{6}He, ^{9}Be(t,α)^{8}Li, ^{10}B(t,p)^{12}B, and ^{11}B(d,p)^{12}B. If lithium is allowed in a target capsule, then ^{6}Li(t,p)^{8}Li and ^{7}Li(t,α)^{6}He would also be included in this list.

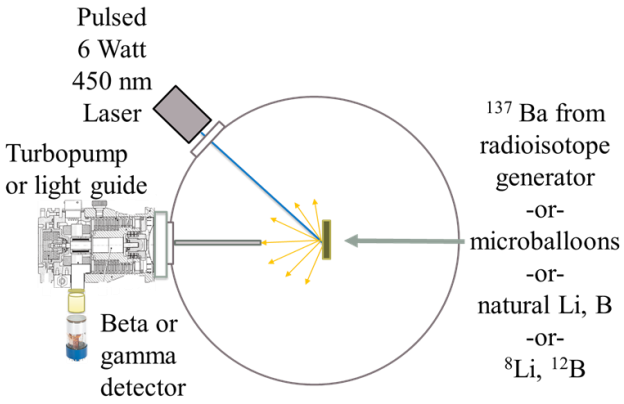

Figure 17. Possible ideas for future tests. Pulses of gas could be introduced into the chamber by letting the laser vaporize: (1) a film of ^{137}Ba created using a ^{137}Cs radioisotope generator, or (2) a real ICF target capsule or microballoons filled with gas, or (3) the surface layer of a target compound containing natural lithium or boron, or (4) ^{8}Li or ^{12}B created using a deuteron beam at SUNY Geneseo via the ^{7}Li(d,p)^{8}Li or ^{11}B(d,p)^{12}B reaction, respectively. Gas could be trapped using (1) the gas collection tube followed by a turbopump or (2) a turbopump simply attached to the chamber, or (3) a getter attached to a detector and inserted near the target.

In addition to continuing the experiments already underway using ^{41}Ar as a longer-lived inert radioactive gas substitute for ^{6}He and using the fast ion gauges to measure the flow of gas and the fraction captured, the following are other possible ideas.

Experiment 1 – A Cs-137/Ba-137m isotope generator could be used to produce a ^{137}Ba solution, having a half-life of 2.6 min. This solution could be quickly evaporated onto a substrate, and then quickly inserted into the center of the vacuum chamber through an airlock. A pulsed 6 W laser beam that strikes the ^{137}Ba residue would vaporize it. The ^{137}Ba nuclei would be either collected and trapped by the turbopump or by a getter, and counted by a gamma ray detector. This experiment would allow comparison of the effectiveness of the two proposed methods for capturing a chemically reactive isotope.

Experiment 2 – Microballoons, or better yet, an actual ICF target capsule in the center of the chamber could be filled with helium gas by filling the chamber with helium, allowing time for the helium to permeate the capsule walls, then quickly pumping down the chamber before the gas escapes from the capsule. Hitting the target capsule with the laser would hopefully release the gas in an isotropic expansion. The distribution could be measured using the fast ion gauges, and a fast ion gauge in the foreline trap could be used to determine the fraction of the released gas that is collected.

Experiment 3 – Laser pulses could be allowed to strike elemental lithium or boron or compounds containing these natural elements, possibly vaporizing a small amount which could then be collected in the turbopump trap or more likely on a getter.

Experiment 4 – Deuterons from the SUNY Geneseo Pelletron accelerator could be allowed to strike a natural lithium (95% ^{7}Li) target, creating ^{8}Li via ^{7}Li(d,p)^{8}Li, or a natural boron target (80% ^{11}B) creating ^{12}B via ^{11}B(d,p)^{12}B. Both of these reactions have a cross section of 0.2 b at 3 MeV. The deuteron beam itself may heat the surface enough for these atoms to fly off, or the laser could be used to further heat the surface. Experiments to see whether these atoms can be collected and detected could be carried out.

Conclusion and future plans

We have designed and built an experimental testbed for studying the release, capture and detection of both inert and chemically reactive radioactive gases. This test system includes a fast valve for releasing gas and fast ion gauges for measuring changes in pressure, both on the 100 μs time scale. It includes a turbopump trap and detector system for detecting trapped radioactive nuclei. Using the SUNY Geneseo Pelletron we are developing methods for producing radioactive gases that can be released into the test system, including ^{41}Ar which has already been created and detected.

In the future months we hope to successfully transport the ^{41}Ar to Houghton, inject it into the vacuum chamber, capture it with the turbopump and detect both beta particles and gamma rays, measuring both their energy spectra and decay curves. We plan to work toward carrying out the experiments above, which are listed in order of increasing difficulty. In order to do this, we will need to design and build a large solid angle phoswich detector that can be attached to the turbopump foreline. We also will need to design and build a phoswich detector that can be covered with a getter and inserted into the vacuum chamber.

Presentations made since summer 2017

Micah Coats, Katelyn Cook, Mark Yuly, Stephen Padalino, Craig Sangster and Sean Regan. "A Phoswich Detector System to Measure Sub-Second Half-Lives using ICF Reactions"

1. Omega Laser User's Group Meeting, Laboratory for Laser Energetics, Rochester, NY, April 25, 2018.
2. 2018 Omega Laser Facility Users Group Workshop Student Poster Award.
3. XXXVII Annual Rochester Symposium for Physics Students, SUNY Brockport, Brockport, NY., April 7, 2018
4. 59th Annual Meeting of the APS Division of Plasma Physics, Milwaukee, WI, Oct. 23-27, 2017.
5. 2017 APS Division of Plasma Physics Outstanding Undergraduate Poster Award.

This material is based upon work supported by the Department of Energy [National Nuclear Security Administration] University of Rochester "National Inertial Confinement Program" under Award Number(s) DE-NA0004144.

[1] C. Stoekl et al., Rev. Sci. Instrum. **87**, 053501 (2016).
[2] B. M. Sherrill et al., Nucl. Instrum. Methods **A 432**, 299 (1999).
[3] G. W. Hitt et al., Nucl. Instrum. Methods **A 566**, 264 (2006).
[4] S. Brandenburg *et al.*, in *Cyclotrons and Their Applications 2001*, proceedings of the 16th International Conference on Cyclotrons and Applications, edited by F. Marti (American Institute of Physics, 2001), p. 463.
[5] National Nuclear Data Center, information extracted from the Chart of Nuclides database, http://www.nndc.bnl.gov/chart/.
[6] H. S. Bosch and G. M. Hale, Nucl. Fusion **32** 611 (1992)
[7] S.N. Abramovich, B.Ya. Guzhovskij, V.A. Zherebtsov, and A.G. Zvenigorodskij, International Nuclear Data Committee Report INDC(CCP)-326/L+F, (1991).
[8] A.J. Koning, S. Hilaire and M.C. Duijvestijn, "TALYS-1.0", Proceedings of the International Conference on Nuclear Data for Science and Technology, April 22-27, 2007, Nice, France, editors. O.Bersillon, F.Gunsing, E.Bauge, R.Jacqmin, and S.Leray, EDP Sciences, 2008, p. 211-214.
[9] G.M. Hale and D. C. Dodder, Proceedings of the International Conference on Nuclear Cross Sections for Technology, NBS Special Publication 594 (1979) (Los Alamos Report LA-UR-79-2896).
[10] D. Ciric,B. Stepancic,R. Popic,D. Stanojevic, and M. Aleksic, Fizika **4**, 193 (1972).
[11] F. E. Cecil et al., Phys. Rev. C 27, 6 (1983).
[12] D. Ciric,B. Stepancic,R. Popic,D. Stanojevic, and M. Aleksic, Fizika **4**, 193 (1972).
[13] K.S.Nam and G.M.Osetinskii Yadernaya, Fizika **9**, 487 (1969) (Soviet Journal of Nuclear Physics **9**, 279 (1969), USA).
[14] R.W. Kavanagh and C.A. Barnes, Phys. Rev. **112**, 503 (1958).
[15] N.A. Bostrom,E.L. Hudspeth, and I.L. Morgan, Phys. Rev. **105**, 1545 (1957).

[16] M. A. Stoyer, C. A. Velsko, B. K. Spears, D. G. Hicks, G. B. Hudson, T. C. Sangster, and C. G. Freeman, Rev. Sci. Instrum. **83**, 023505 (2012).
[17] T. E. Weber and T. P. Intrator, Rev. .Sci. Instrum. **85**, 043501 (2014).